NANO · MICRO small
www.small-journal.com

Ultrathin MXene Nanosheets Decorated with TiO_2 Quantum Dots as an Efficient Sulfur Host toward Fast and Stable Li–S Batteries

Xiao-Tian Gao, Ying Xie, Xiao-Dong Zhu, Ke-Ning Sun, Xu-Ming Xie, Yi-Tao Liu,* Jian-Yong Yu, and Bin Ding*

Being conductive and flexible, 2D transition metal nitrides and carbides (MXenes) can serve in Li–S batteries as sulfur hosts to increase the conductivity and alleviate the volume expansion. However, the surface functional groups, such as −OH and −F, weaken the ability of bare MXenes in the chemisorption of polysulfides. Besides, they create numerous hydrogen bonds which make MXenes liable to restack, resulting in substantial loss of active area and, thus, inaccessibility of ions and electrolyte. Herein, a facile, one-step strategy is developed for the growth of TiO_2 quantum dots (QDs) on ultrathin MXene ($Ti_3C_2T_x$) nanosheets by cetyltrimethylammonium bromide-assisted solvothermal synthesis. These QDs act as spacers to isolate the MXene nanosheets from restacking, and preserve their 2D geometry which guarantees larger electrode–electrolyte contact area and higher sulfur loading. The stronger adsorption energy of polysulfides with TiO_2 (than with $Ti_3C_2T_x$), as proven by density functional theory calculations, is essential for better on-site polysulfide retention. The ultrathin nature and protected conductivity ensure rapid ion and electron diffusion, and the excellent flexibility maintains high mechanical integrity. In result, the TiO_2 QDs@MXene/S cathode exhibits significantly improved long-term cyclability and rate capability, disclosing a new opportunity toward fast and stable Li–S batteries.

Nowadays, the global interest in green cars, arising from our worries on the increasingly serious emission problem, results in an urgent need for next-generation battery systems with higher energy and power densities. Li-ion batteries based on an intercalation mechanism are willing but unable to meet this requirement. In this circumstance, Li–S batteries based on a multielectron chemical reaction become a promising candidate due to extremely high theoretical capacity (1675 mA h g^{-1}) and energy density (2600 W h kg^{-1}) of the sulfur cathode.[1] Besides, sulfur is naturally abundant and environmentally friendly. Unfortunately, Li–S batteries currently suffer from rapid capacity decay, poor rate capability, and low coulombic efficiency due to three inherent deficiencies: (i) the low conductivity of sulfur (5×10^{-30} S cm^{-1}) as well as its discharging products (Li_2S_2/Li_2S) which leads to limited utilization of the cathode material; (ii) the shuttling of the intermediate polysulfides, generated during repeated charging/discharging, from cathode to anode which brings about continuous consumption of the cathode material; (iii) the considerable volume expansion (>80%) of sulfur which causes destruction of the mechanical integrity.

To partially address these issues, researchers tried to host sulfur by various carbonaceous materials, for example, porous

X.-T. Gao, Prof. Y.-T. Liu, Prof. J.-Y. Yu, Prof. B. Ding
Innovation Center for Textile Science and Technology
Donghua University
Shanghai 200051, China
E-mail: liu-yt03@mails.tsinghua.edu.cn
X.-T. Gao
School of Chemistry and Chemical Engineering
Harbin Institute of Technology
Harbin 150001, China
Prof. Y. Xie
Key Laboratory of Functional Inorganic Material Chemistry (Ministry of Education)
School of Chemistry and Materials Science
Heilongjiang University
Harbin 150080, China
The ORCID identification number(s) for the author(s) of this article can be found under https://doi.org/10.1002/smll.201802443.
Prof. X.-D. Zhu, Prof. K.-N. Sun
Academy of Fundamental and Interdisciplinary Sciences
Harbin Institute of Technology
Harbin 150080, China
E-mail: zxd9863@163.com
Prof. X.-M. Xie
Key Laboratory of Advanced Materials (Ministry of Education)
Department of Chemical Engineering
Tsinghua University
Beijing 100084, China

DOI: 10.1002/smll.201802443

carbons,[2] hollow carbon spheres,[3] carbon nanotubes (CNTs),[4] and carbon nanofibers,[5] thereby increasing the conductivity and alleviating the volume expansion. However, the nonpolar, hydrophobic carbonaceous materials could hardly trap the polar, hydrophilic polysulfides due to their weak interactions, so the shutting problem remained unsolved. In this context, reduced graphene oxide (r-GO) emerged as a sulfur host since its oxygen moieties could confine polysulfides through chemisorption to some extent.[6] Recently, a new class of inorganic graphene analogues, that is, MXenes including transition metal carbides and nitrides, has joined the huge family of 2D materials.[7] Structurally, MXenes resemble GO in that they possess plenty of functional groups, such as −OH and −F, on the surface.[8] Whereas, different from GO whose conductivity is completely destroyed due to severe structural distortions, MXenes are much more conductive than solution-processed r-GO films.[9] Because of these fascinating characteristics, great expectations are placed on MXenes to compete with r-GO in versatile applications.[10]

Exfoliated MXene was first employed as a substitute for r-GO to host sulfur by Nazar and co-workers and Wang and co-workers.[11] Being conductive and flexible,[9,12] MXene nanosheets could increase the conductivity as well as accommodate the volume expansion of the loaded sulfur particles. At the same time, their polar, hydrophilic surface laid a basis for the chemisorption of polysulfides in a moderate degree. Unfortunately, one insurmountable barrier faced by MXene nanosheets was their strong tendency to restack due to numerous hydrogen bonds created by the surface functional groups, resulting in substantial loss of active area and, thus, inaccessibility of ions and electrolyte. Therefore, the long-term cyclability and rate capability of the MXene/S cathode were not satisfactory. As such, they introduced mesoporous carbon, r-GO, or CNTs to isolate MXene nanosheets before sulfur loading.[13] On the other hand, polar metal oxides such as TiO_2 were reported to be strong polysulfide adsorbents.[14] However, in view of its inferior Li-ion diffusivity ($\approx 10^{-12}$ to 10^{-9} cm^2 s^{-1}) and conductivity ($\approx 10^{-12}$ to 10^{-7} S cm^{-1}), TiO_2 alone was not sufficient as a sulfur host. In this respect, a small amount of TiO_2 was grown on r-GO nanosheets, which exhibited a synergistic effect on both polysulfide confinement and conductivity enhancement.[15]

Inspired by these results, and bearing the unique merits and drawbacks of MXenes in mind, we envision constructing a hybrid architecture, consisting of TiO_2 decorated MXene nanosheets, as a high-performance sulfur host. Hybridizing 2D MXenes with low-dimensional TiO_2 in a well-defined architecture is, however, a huge challenge still beyond the reach of the state-of-the-art techniques.[16] The very reason lies in the poor oxygen resistance of MXenes, originating from the exposure of a large portion of metal atoms on the surface,[17] which makes them liable to be oxidized by oxygen dissolved in aqueous solutions.[18] Therefore, the hydrothermal route which was used to synthesize TiO_2/r-GO nanohybrids is invalid on MXenes.[19] Previously, we reported a two-step route to the self-assembly of presynthesized metal oxide nanostructures on MXene nanosheets in a nonsolvent by van der Waals attraction.[20] However, its yield was relatively low due to the poor dispersibility of MXene nanosheets in this nonsolvent.

Here we report, for the first time, a facile, one-step strategy for the growth of TiO_2 quantum dots (QDs) on ultrathin MXene ($Ti_3C_2T_x$) nanosheets through cetyltrimethylammonium bromide (CTAB)-assisted solvothermal synthesis. This strategy can well protect MXene from oxidation due to the presence of CTAB, so the resulting TiO_2 QDs@MXene nanohybrids are highly conductive. We highlight the following superiorities of our TiO_2 QDs@MXene nanohybrids over neat MXene nanosheets as a sulfur host: First of all, TiO_2 QDs are uniformly decorated on MXene nanosheets, acting as spacers to prevent them from restacking and preserve their 2D geometry. The well-preserved 2D geometry therefore guarantees larger electrode–electrolyte contact area and higher sulfur loading.[11,21] Second, the stronger adsorption energy of polysulfides with TiO_2 than with $Ti_3C_2T_x$ (which is weakened by the surface functional groups) is essential for better on-site polysulfide retention, and helps to reduce the polarization of the sulfur cathode especially at high rates.[22] Third, the ultrathin nature together with the protected conductivity ensures rapid ion and electron diffusion. Last but not least, the excellent mechanical flexibility maintains high integrity during repeated charging/discharging. As a result, the TiO_2 QDs@MXene/S cathode exhibits significantly improved long-term cyclability and rate capability without needing any sophisticated post treatment, such as electrolyte/binder optimization or physical interlayer, and discloses a new opportunity toward fast and stable Li–S batteries.

The whole process for synthesizing the TiO_2 QDs@MXene nanohybrids is illustrated in **Figure 1**. Ti_3AlC_2 is a typical ternary carbide with a layered structure, and is a precursor for preparing MXene ($Ti_3C_2T_x$) nanosheets by selectively etching the Al layers with LiF/HCl.[23] Due to the exposure of a large portion of metal atoms on the surface, these nanosheets are thermodynamically unstable, and suffer from poor oxygen resistance under hydrothermal conditions.[17] Once oxidized, MXene is partially or completely converted to TiO_2, and its morphology and conductivity are seriously impaired.[18] Here, we adopt a CTAB-assisted solvothermal strategy for the growth of TiO_2 QDs on MXene nanosheets. Fundamentally, an aqueous solution of MXene is mixed with an *n*-hexane/*n*-pentanol solution of CTAB, and MXene nanosheets will be surrounded by water droplets under the assistance of CTAB in this water-in-oil (W/O) emulsion. Then Ti^{3+} ions are added as a titanium source, and they will be spontaneously anchored to the negatively charged functional groups of MXene through electrostatic attraction, where they nucleate, crystallize, and grow into TiO_2 QDs. All these stages are carried out in the confined nanoscale water pools of the W/O emulsion.[24] Due to the presence of CTAB as a surfactant, MXene nanosheets are well protected from oxidation, and the conductivity of a vacuum-filtered TiO_2 QDs@MXene film is up to 3.7×10^2 S cm^{-1} under four-probe measurement. This value is significantly higher than the conductivity of r-GO, which varies from 0.17 to 3.05 S cm^{-1} (reduced by sodium borohydride),[25] 20 S cm^{-1} (reduced by aluminum powder),[26] 26.9 to 77 S cm^{-1} (reduced by vitamin C),[27] 41 to 99 S cm^{-1} (reduced by hydrazine hydrate).[27] Next, S_8 molecules are fixed on the TiO_2 QDs@MXene nanohybrids through chemisorption, resulting in a TiO_2 QDs@MXene/S cathode for the following electrochemical tests.

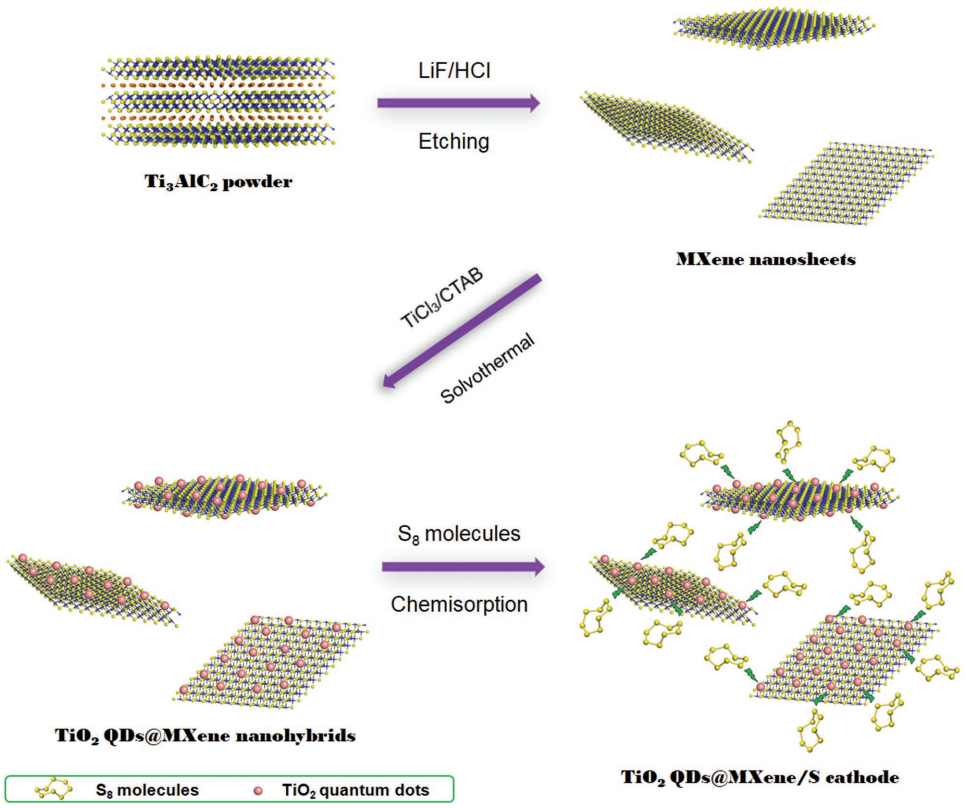

Figure 1. Schematic illustration of the preparation of MXene ($Ti_3C_2T_x$) nanosheets from Ti_3AlC_2 by LiF/HCl etching, the growth of TiO_2 QDs on MXene nanosheets by CTAB-assisted solvothermal synthesis, as well as the fabrication of TiO_2 QDs@MXene/S cathode by chemisorption of S_8 molecules.

Figure 2a shows a transmission electron microscopy (TEM) image of the MXene nanosheets, which have a flat and smooth surface, and are folded due to high flexibility and elasticity. An atomic force microscopy (AFM) image of the MXene nanosheets is given in Figure S1 (Supporting Information), which reveals a thickness of <2 nm corresponding to one or two layers on a substrate.[28] In contrast, the surface of the TiO_2 QDs@MXene nanohybrids is decorated with the TiO_2 QDs, as shown in Figure 2b. These nanohybrids are nearly transparent to the electron beam, which demonstrates their ultrathin nature. Besides, they are well isolated from each other due to the presence of TiO_2 QDs as spacers. Figure S2 (Supporting Information) displays large-area TEM and scanning electron microscopy (SEM) images of the TiO_2 QDs@MXene nanohybrids, from which we can see the distribution of TiO_2 QDs is very uniform, indicating fairly high efficiency and yield of our strategy. Under high-resolution TEM (HRTEM) observation (Figure 2b, inset), the lattice fringe spacing is measured to be 0.35 nm, which is in good agreement with the (101) plane of anatase TiO_2.[24] Figure S3 (Supporting Information) shows the size distribution of 200 individual TiO_2 QDs, which reveals an average diameter of 4.3 nm falling well within the QD range. The TiO_2 content is controlled to be <10 wt%, since too much TiO_2 will offset the positive effect due to its extremely low Li-ion diffusivity and conductivity. Note that when CTAB is absent, MXene nanosheets will be oxidized under the same conditions. Different from the TiO_2 QDs@MXene nanohybrids, the oxidized MXene nanosheets have a loose and porous structure, and are composed of a number of small crystallites of TiO_2 (Figure S4, Supporting Information). These TiO_2 crystallites are irregular in morphology, with sizes of dozens of nanometers, which are in consistent with previous reports.[18]

Figure 2c shows the X-ray diffraction (XRD) pattern of the MXene nanosheets, which has diffraction peaks assigned to the (002), (004), (006), (008), (0010), and (0012) planes of $Ti_3C_2T_x$.[29] As to the XRD pattern of the TiO_2 QDs@MXene nanohybrids (Figure 2d), a combination of the (002) peak of MXene with the (101), (004), (200), (105), (211), (204), (116), and (215) peaks of anatase TiO_2 (JCPDS Card No. 21-1272) can be observed. The presence of MXene's (002) peak, in contrast to the case of hydrothermal synthesis where it vanished,[17] demonstrates that the MXene nanosheets are well protected and suffer from little, if any, structural degradation by our CTAB-assisted solvothermal method. Conversely, the XRD pattern of the oxidized MXene nanosheets shows peaks characteristic of a mixture of anatase and rutile TiO_2 (Figure S5, Supporting Information). The Ti 2p X-ray photoelectron spectroscopy (XPS) spectrum of the MXene nanosheets is provided in Figure 2e, which displays the Ti—C, Ti^{2+}, and Ti^{3+} peaks that are in good agreement with our previous report.[20] There are no peaks deconvoluted for TiO_2, indicating the MXene nanosheets were not oxidized during synthesis. As to the XPS spectrum of the TiO_2 QDs@MXene nanohybrids (Figure 2f), peaks assigned to Ti—C, Ti^{2+}, and Ti^{3+} are observed, which are similar to those of the MXene nanosheets. Besides, two more peaks, that is, Ti—O sp^3 and sp^1 peaks occur, which originate from TiO_2 QDs. This is

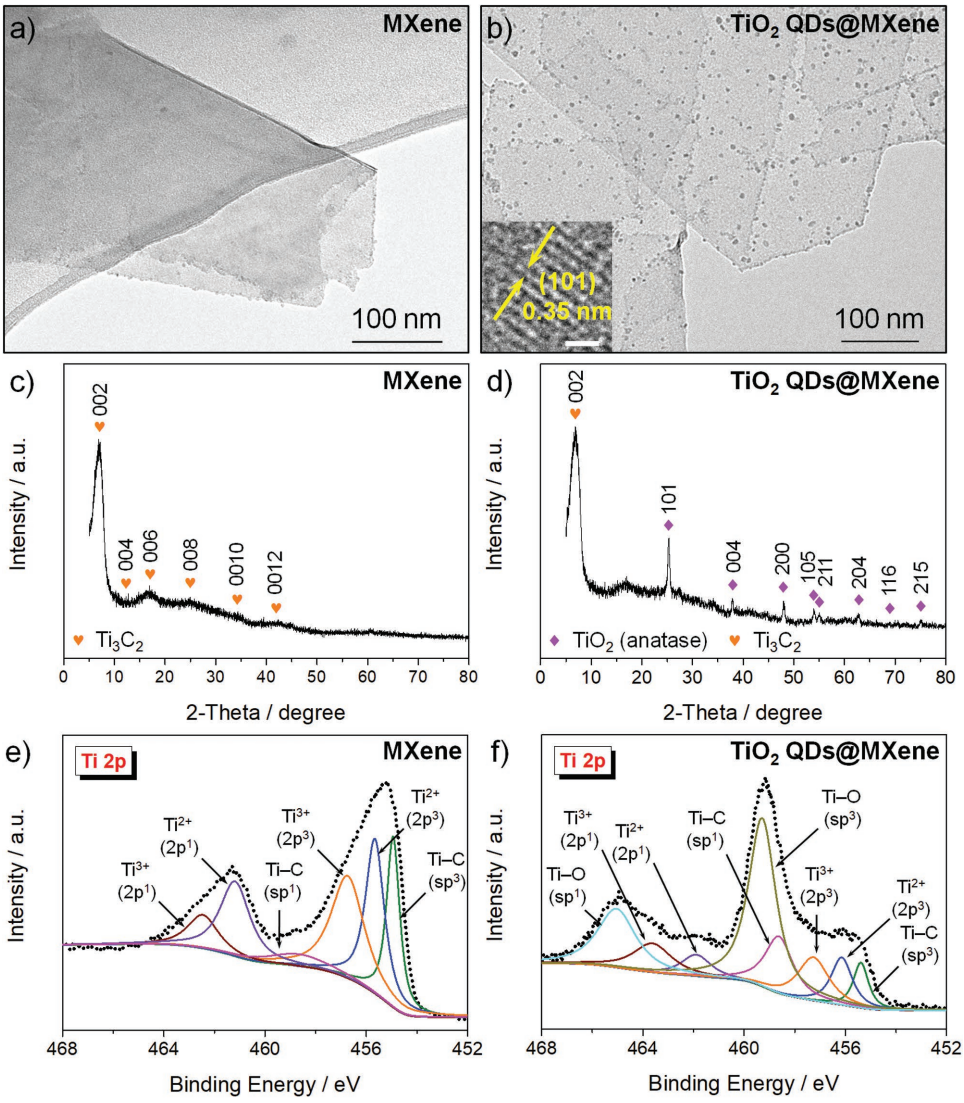

Figure 2. a,b) TEM images, c,d) XRD patterns, and e,f) Ti 2p XPS spectra of MXene nanosheets and TiO_2 QDs@MXene nanohybrids, respectively. The inset in (b) shows an HRTEM image of TiO_2 QDs decorated on MXene nanosheets (scale bar = 1 nm).

significantly different from the XPS spectrum of the oxidized MXene nanosheets, where only the Ti—O (sp^1 and sp^3) peaks are observed (Figure S6, Supporting Information).[30]

An SEM image of the TiO_2 QDs@MXene/S cathode, fabricated by melt diffusion of sulfur (≈80 wt%, Figure S7, Supporting Information) into the TiO_2 QDs@MXene nanohybrids, is presented in **Figure 3**a. The corresponding energy-dispersive X-ray spectroscopy (EDS) reveals homogeneous elemental distribution of C, Ti, O, and S, demonstrating that the sulfur particles are homogeneously loaded on the well-isolated, ultrathin TiO_2 QDs@MXene nanohybrids without obvious agglomeration. The XRD pattern (Figure 3b) of the TiO_2 QDs@MXene/S cathode discloses, besides the well-indexed MXene (002) plane, a number of sharp peaks arising from highly crystalline orthorhombic sulfur (JCPDS Card No. 08-0247). It needs to be emphasized that in addition to the role of spacers in isolating the MXene nanosheets physically, TiO_2 QDs also serve as adsorbents to confine polysulfides chemically.[14] To elucidate the nature of this chemisorption, simulations based on density functional theory (DFT) are conducted by using the Vienna Ab Initio Simulation Package (VASP).[31] The computational details are provided in the Experimental Section, and the optimized structures of a representative polysulfide, that is, Li_2S_4, on different surfaces are depicted in Figure 3c. Figure 3d displays the adsorption energies of Li_2S_4 on different surfaces. Our results clearly demonstrate that a strong chemical interaction (–13.91 eV) is formed between Li_2S_4 and bare MXene (Ti_3C_2), suggesting that bare MXene is an excellent material for stabilizing polysulfides. However, the exfoliation of Ti_3AlC_2 by selectively etching the Al layers with LiF/HCl inevitably induces plenty of surface functional groups, such as —OH and —F. Our calculations further identify that the saturation of MXene by —OH and —F leads to significantly decreased adsorption energies of –2.62 and –0.29 eV, respectively. Therefore, such a screening effect will hinder the fixation of polysulfides on MXene's surface, which is also supported

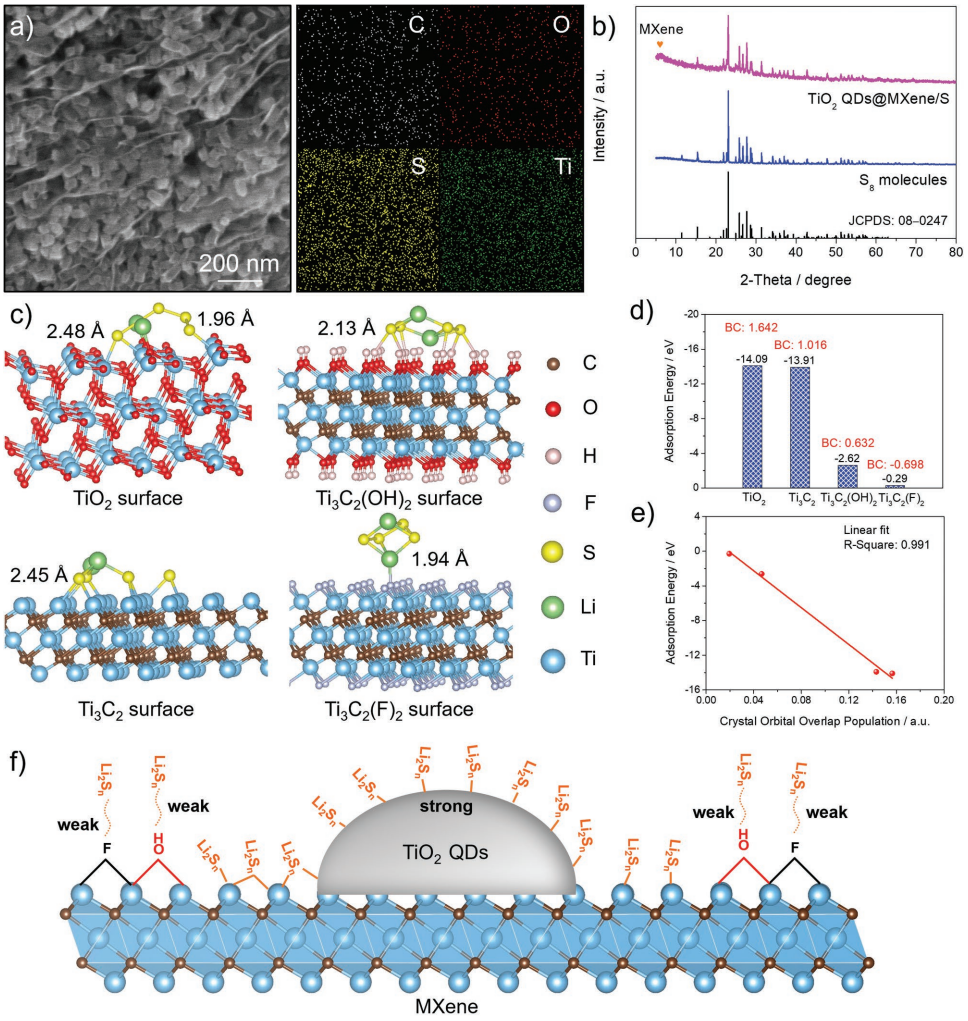

Figure 3. a) SEM image and the corresponding EDS maps, and b) XRD pattern of TiO_2 QDs@MXene/S cathode; c) optimized structures of Li_2S_4 adsorbed on TiO_2, Ti_3C_2, $Ti_3C_2(OH)_2$, and $Ti_3C_2(F)_2$ surfaces; d) adsorption energies of Li_2S_4 on different surfaces; e) linear fit between adsorption energy and COOPs; f) strategy for suppressing the shuttling effect of polysulfides by the growth of TiO_2 QDs on MXene nanosheets.

by others' calculations.[32] The reason for this phenomenon is related to the electronic structures of different surfaces, and the Bader charge (BC) analysis confirms that the F species on the $Ti_3C_2(F)_2$ surface possess a negative value (–0.698 e). According to the electrostatic consideration, the S species in polysulfides are very difficult to be attached to the $Ti_3C_2(F)_2$ surface. Even if the S species contact the $Ti_3C_2(F)_2$ surface in the initial configuration, Li—F bonds (1.94 Å) are formed preferentially between them after geometry optimization. As to the $Ti_3C_2(OH)_2$ surface, the change of the surface status with respect to $Ti_3C_2(F)_2$ leads to stronger chemical bonds between the S(Li) and H species on the $Ti_3C_2(OH)_2$ surface. Therefore, the adsorption energy (–2.62 eV) of Li_2S_4 on the $Ti_3C_2(OH)_2$ surface is improved slightly.

To estimate the bonding strength between Li_2S_4 and different surfaces, the crystal orbital overlap populations (COOPs), a powerful bonding descriptor constructed by generating an overlap population-weighted density of states (DOS) on a specific bond, are calculated and depicted in Figure 3e.[33] The results show that a perfect linear relationship exists between the adsorption energy and the interfacial bonding, and that the performance of different materials depends on their surface status. Therefore, a feasible strategy for suppressing the shuttling effect of polysulfides is illustrated in Figure 3f. Although exposing bare MXene surface by preventing the creation of surface functional groups during synthesis is helpful, this strategy is very difficult in reality. So the introduction of TiO_2 QDs on MXene to replace the passivation layer is alternatively feasible and effective, which is confirmed by the calculated adsorption energy (–14.09 eV) in Figure 3d. Furthermore, since the size of TiO_2 QDs is very small (<5 nm), the recovery of the polysulfides fixation ability of MXene does not sacrifice its energy density. The TiO_2 QDs@MXene nanohybrids thus exhibit excellent performance on suppressing the shuttling effect of polysulfides, resulting in superior long-term cyclability and rate capability as will be proven by the electrochemical results.

The first three cyclic voltammetry (CV) curves of the TiO_2 QDs@MXene/S and MXene/S cathodes, in the voltage range of 1.5–3.0 V at a scan rate of 0.2 mV s^{-1}, are shown in Figures S9 and S10 (Supporting Information), and the

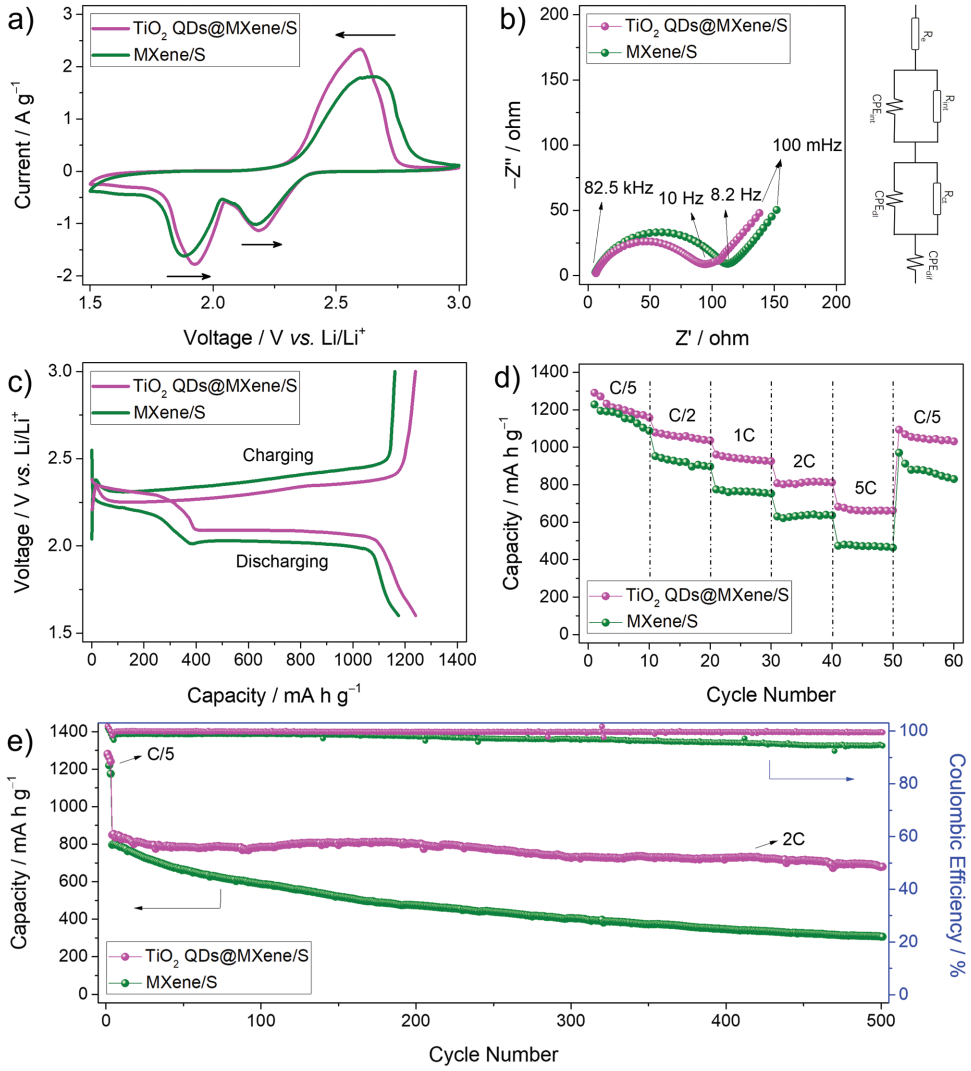

Figure 4. Comparisons of a) third CV curves (scan rate = 0.2 mV s^{-1}), b) Nyquist plots after third cycle, c) third charging/discharging curves at C/5, d) rate capabilities, and e) cycle behaviors at 2C (sulfur loading = 1.5 mg cm^{-2}) of TiO_2 QDs@MXene/S and MXene/S cathodes (1C = 1675 mA g^{-1}). The inset in (b) shows the equivalent circuit model.

comparison of the third CV curves is given in **Figure 4**a. Both cathodes exhibit two reduction peaks and one oxidation peak, which are associated with the transformation of elemental sulfur and lower-order lithium sulfides.[14e] The reduction peak at the higher voltage (φ_{c1}) is related to the reduction of elemental sulfur to higher-order polysulfides (Li_2S_n, $4 \le n \le 8$), while the reduction peak at the lower voltage (φ_{c2}) is assigned to the reduction of higher-order polysulfides to lower-order lithium sulfides (Li_2S_2/Li_2S).[11b,13a] The potentials of these reduction and oxidation peaks are listed in Table S1 (Supporting Information). The potential differences (0.41 and 0.67 V) between the reduction and oxidation peaks of the TiO_2 QDs@MXene/S cathode are lower than those (0.48 and 0.77 V) of the MXene/S cathode, suggesting smaller polarization of the former.

These results are in consistent with the electrochemical impedance spectra (EIS), as shown in Figure 4b. As shown in Figure S11 (Supporting Information), by using the equivalent circuit proposed by Deng et al.,[34] the fitted impedance plots agree well with the actual impedance spectra. The fitting results of the two cathodes are given in Table S2 (Supporting Information). In the proposed circuit model, R_e is the ohmic resistance mainly resulting from the electrolyte as well as the other parts of the cell, corresponding to the intercept with the real axis at the high frequency. The semicircle in the high–medium frequency region is really coupled by a high-frequency arc (R_{int}//CPE_{int}) and a medium-frequency arc (R_{ct}//CPE_{dl}). R_{int}//CPE_{int} is the interface contact resistance and its related capacitance in the bulk cathode, which simulates the process of electron conduction from the current collector to the reaction sites. R_{ct}//CPE_{dl} is the charge-transfer resistance and its related capacitance, which reflects the charge transfer process at the interface between the reaction sites and the electrolyte. CPE_{dif} is the diffusion impedance that probably represents the Li-ion diffusion process through the bulk electrode. The impedance of CPE, Z_{CPE}, is defined as

$$Z_{CPE} = Y^{-1}(jw)^{-n} \quad (1)$$

When n = 1, CPE reduces to an ideal capacitor with the capacitance Y; when n = 0, CPE reduces to a simple resistor with the admittance Y.

As seen from Table S2 (Supporting Information), the introduction of TiO_2 QDs does not fundamentally affect the ohmic resistance (5.44 vs 4.84 Ω). However, more or less, the presence of TiO_2 QDs obstructs the electron conduction from the current collector to the reaction sites, resulting in an increase of the interface contact resistance from 17.95 to 21.80 Ω. Note that the much lower charge-transfer resistance of the TiO_2 QDs@MXene/S cathode than the MXene/S cathode (76.24 vs 97.62 Ω) is beneficial for the enhancement of the charge transfer kinetics. This is because that TiO_2 QDs can effectively trap more polysulfides and bring more active sites onside the reaction interface.

Figure 4c compares the third charging/discharging curves of the TiO_2 QDs@MXene/S and MXene/S cathodes. As seen from this figure, each discharging curve possesses two obvious plateaus, which correspond to the multistep reduction reaction of sulfur during the discharging process.[35] The plateau at the higher voltage (2.38–2.09 V for TiO_2 QDs@MXene/S, and 2.31–2.03 V for MXene/S) is ascribed to the reduction of elemental sulfur to higher-order polysulfides (Li_2S_n, $4 \le n \le 8$), while the plateau at the lower voltage (≈2.09 V for TiO_2 QDs@MXene/S, and ≈2.03 V for MXene/S) is associated with the reduction process of higher-order polysulfides to lower-order lithium sulfides (Li_2S_2/Li_2S).[11b] In contrast, the charging curve ascends slowly in the voltage range of 2.15–2.28 V for TiO_2 QDs@MXene/S (2.21–2.35 V for MXene/S). The potential differences between the charging and discharging plateaus of the TiO_2 QDs@MXene/S cathode are 0.06–0.10 V lower than those of the MXene/S cathode, also suggesting smaller polarization of the former. This result is in good agreement with the phenomenon observed in the CV comparison (Figure 4a). Besides, the discharging plateau at the lower voltage of the TiO_2 QDs@MXene/S cathode is much longer than that of the MXene/S cathode, which is a direct proof that TiO_2 QDs can effectively adsorb [S_4^{2-}] to suppress their diffusion. Therefore, more [S_4^{2-}] are converted to Li_2S_2/Li_2S, thus increasing the discharging capacity significantly.

To testify the superiority of the TiO_2 QDs@MXene/S cathode over MXene/S in terms of rate capability, they were cycled at different rates, as shown in Figure 4d. Apparently, the former delivers capacities as high as 1158, 1037, 925, 812, and 663 mA h g^{-1} at C/5, C/2, 1C, 2C, and 5C (1C = 1675 mA g^{-1}). When the current density is relaxed to C/5, the capacity returns to 1031 mA h g^{-1} after ten cycles, demonstrating very good reversibility and stability. In contrast, the capacities of the MXene/S cathode are only 1088, 897, 753, 636, and 464 mA h g^{-1} at the same rates. The long-term cyclability of the TiO_2 QDs@MXene/S cathode, especially at a high rate, is displayed in Figure 4e. As expected, a strikingly high capacity of 680 mA h g^{-1} is delivered at 2C after 500 cycles (sulfur loading = 1.5 mg cm^{-2}), which is more than twice that (308 mA h g^{-1}) of the MXene/S cathode. The capacity retention of the TiO_2 QDs@MXene/S cathode is as high as 80%,

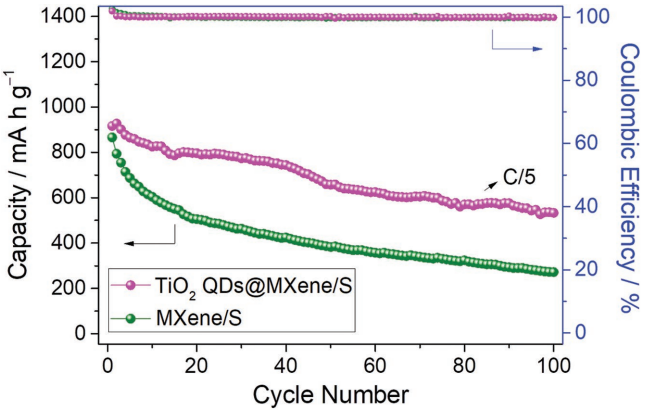

Figure 5. Comparisons of cycle behaviors at C/5 (sulfur loading = 5.5 mg cm^{-2}) of TiO_2 QDs@MXene/S and MXene/S cathodes.

corresponding to a decay rate of only 0.04% $cycle^{-1}$. Besides, the coulombic efficiency of the TiO_2 QDs@MXene/S cathode is nearly 100% throughout the whole cycling process, while that of the MXene/S cathode decreases gradually at the later stage of the cycling process. This phenomenon indicates that the relatively weak interactions between polysulfides and MXene cannot effectively solve the shuttling problem, thus making the charging capacity much lower than the discharging capacity.

Note that a high sulfur loading (>5 mg cm^{-2}) is a key factor for high-energy-density batteries. Therefore, both TiO_2 QDs@MXene/S and MXene/S cathodes were cycled at C/5 at a sulfur loading of 5.5 mg cm^{-2}, as shown in **Figure 5**. Similarly, the former delivers a capacity of 533 mA h g^{-1} corresponding to a capacity retention of 58%, both of which are significantly higher than those (272 mA h g^{-1}, 31%) of the latter. It should be noted, however, that the cycle stability is not so good as that at a lower mass loading of sulfur (Figure 4e). This is mainly because a higher mass loading results in a thicker electrode film and, thus, stronger polarization. Therefore, the discharging performance of the cell declines. The coulombic efficiency also decreases, resulting in weaker capacity retention.

The greater electrochemical performance of the TiO_2 QDs@MXene/S cathode can be understood from the fact that MXene nanosheets tend to restack after exfoliation, which seems to limit the accessibility of ions and electrolyte, thus hindering the full utilization of their surfaces. Things are made worse since their surface functional groups, such as —OH and —F, are not favorable for fixing the polysulfides and suppressing the shutting effect as compared to bare MXenes. All these deficiencies can be perfectly solved by the presence of TiO_2 QDs, which play a key role in preventing MXene nanosheets from restacking, as well as helping to reduce the polarization at high rates. The better on-site polysulfide retention of the TiO_2 QDs@MXene/S cathode is demonstrated in Figure S12 (Supporting Information). Note that TiO_2 QDs can form Lewis acid–base pairs with sulfur species by involving the unoccupied orbitals of the surface Ti atoms,[36] therefore an obvious color difference occurs between the TiO_2 QDs@MXene/Li_2S_4 and MXene/Li_2S_4 solutions after standing for only 1 h, highlighting the stronger polysulfide adsorption capability of the former. This

result can also be confirmed by the corresponding UV–vis tests (Figure S12, Supporting Information).[37]

In conclusion, we have developed a facile, one-step strategy for the growth of TiO_2 QDs on ultrathin MXene nanosheets by CTAB-assisted solvothermal synthesis. This strategy can well protect MXene from oxidation due to the presence of CTAB, so the resulting TiO_2 QDs@MXene nanohybrids are highly conductive. As a sulfur host, the TiO_2 QDs@MXene nanohybrids exhibit the following superiorities: First of all, TiO_2 QDs are uniformly decorated on MXene nanosheets, acting as spacers to prevent them from restacking and preserve their 2D geometry. The well-preserved 2D geometry therefore ensures larger electrode–electrolyte contact area and higher sulfur loading. Second, the stronger adosprtion energy of polysulfides with TiO_2 than with MXenes, as proven by DFT calculations, is essential for better on-site polysulfide retention, and helps to reduce the polarization of sulfur cathode especially at high rates. Third, the ultrathin nature together with the protected conductivity ensures rapid ion and electron diffusion. Last but not least, the excellent mechanical flexibility maintains high integrity during repeated charging/discharging. In result, the TiO_2 QDs@MXene/S cathode is superior to the MXene/S cathode in terms of long-term cyclability and rate capability, delivering a strikingly high capacity of 680 mA h g^{-1} at 2C after 500 cycles. We believe this work may disclose a new opportunity toward fast and stable Li–S batteries.

Experimental Section

Preparation of Ti_3AlC_2 Powder: Commercialized Ti_2AlC and TiC were mixed at a molar ratio of 1:1, and ball-milled for 18 h. The milled powder was heated in a tube furnace at a rate of 5 °C min^{-1} under argon protection to 1350 °C, and kept at that temperature for 2 h. The calcined product was then milled, and sieved by a 400 mesh sieve.[28]

Preparation of MXene ($Ti_3C_2T_x$) Nanosheets: LiF (0.99 g) was added to 12 M HCl (10 mL), and stirred for 5 min for complete dissolution. To this solution Ti_3AlC_2 (1 g) was added slowly, and the whole addition time was controlled in a course of 10 min to avoid overheating. The reaction mixture was kept at 35 °C for 24 h under magnetic stirring, washed with deionized water and centrifuged, and the supernatant was discarded. These procedures were repeated until the pH value of the supernatant was ≈6. The solid was filtered by a polytetrafluoroethylene membrane, and vacuum-dried. The obtained $Ti_3C_2T_x$ powder was then added to deionized water at a concentration of 1 mg mL^{-1}, and sonicated under argon protection for 1 h to obtain an aqueous solution.[23]

Solvothermal Synthesis of TiO_2 QDs@MXene Nanohybrids: CTAB (1.4 g) was dissolved in a mixture of *n*-pentanol (5 mL) and *n*-hexane (30 mL). The aqueous solution of MXene nanosheets (5 mL) was then added slowly, and stirred under argon protection for 30 min. $TiCl_3$ (15 wt%, 20 µL) was added under magnetic stirring, and the emulsion was transferred in a Teflon-lined stainless steel autoclave, and kept at 200 °C for 6 h. The solid was collected, washed with deionized water and absolute alcohol to remove CTAB, and vacuum-dried. The TiO_2 content was in the range of 8–10 wt% as determined by measuring the weights of the MXene nanosheets and the TiO_2 QDs@MXene nanohybrids.

Fabrication of TiO_2 QDs@MXene/S Cathode: The TiO_2 QDs@MXene/S cathode was fabricated by a simple melting-diffusion method as reported by us previously.[38] Briefly, the TiO_2 QDs@MXene nanohybrids and sublimed sulfur powder (99.99%, Aladdin S106613) were homogeneously mixed at a weight ratio of 2:8 by milling. The mixture was then transferred in a Teflon-lined stainless-steel autoclave in a glove box filled with argon, and heated at 155 °C overnight.

Electrochemical Tests: The electrodes were prepared by coating the slurry of active material on aluminum foils. The slurry was obtained by mixing the active material, Ketjen Black, and poly(vinylidene fluoride) at a weight ratio of 8:1:1 in *N*-methyl-2-pyrrolidinone. The electrodes were vacuum-dried at 60 °C for 12 h. The 2025 coin-type cells were assembled in an argon-filled glove box with lithium foils as the counter and reference electrodes. The electrolyte was composed of lithium bis(trifluoromethanesulfonyl)imide (LiTFSI) in a solvent of 1,3-dioxolane (DOL) and dimethoxymethane (DME) (volume ratio = 1:1) with 2% $LiNO_3$. The cycle and rate performance was investigated by a Neware battery test system. The CV tests were performed on a CHI 660D electrochemical workstation in a voltage range between 1.5 and 3.0 V. The EIS tests were performed on a PARSTAT 2273 advanced electrochemical system in a frequency range between 100 kHz and 100 mHz with an AC signal amplitude of 10 mV. The electrode system consisted of a TiO_2 QDs@MXene/S or MXene/S working electrode, a lithium foil counter electrode, and a lithium wire reference electrode. To compare the polysulfide adsorption abilities of the TiO_2 QDs@MXene nanohybrids and the MXene nanosheets, a Li_2S_4 solution (10 mmol L^{-1}) was prepared by adding sulfur and Li_2S at a molar ratio of 1:3 in a mixed solvent of DOL/DME (volume ratio = 1:1), followed by vigorous stirring at ambient temperature until the solids were dissolved completely.

Characterizations: TEM was performed by a Hitachi HT7700 microscope operated at an accelerating voltage of 100 kV. HRTEM was performed by a JEOL JEM-2010 microscope operated at an accelerating voltage of 120 kV. SEM was performed by a Hitachi SU8010 microscope operated at an accelerating voltage of 15 kV. AFM was performed by a Shimadzu SPM 9700 microscope in the tapping mode. XRD was performed by a Bruker D8 Advanced X-ray diffractometer with Cu Kα radiation (λ = 0.154 nm). XPS was performed by a Thermo-Scientific K-Alpha spectrometer. TGA was performed by a SDTQ600 analyzer in a temperature range from ambient temperature to 600 °C at a heating rate of 10 °C min^{-1} under N_2 atmosphere. The conductivity was measured by a TRS-9 four-probe meter. UV–vis was performed by a SHIMADZU VU-2450 spectrometer within the wavelength range of 300–900 nm.

Computational Details: All calculations were performed based on DFT by using the VASP.[31] The projector augmented wave (PAW) technique and the Perdew–Burke–Ernzerhof (PBE) functional with a generalized gradient approximation (GGA-PBE) form were applied to deal with the exchange correlation energy of the systems.[39] The energy cutoff of the plane-wave basis set was 400 eV, and a ($2 \times 2 \times 1$) Monkhorst–Pack grid was used for sampling and integration of the Brillouin zone. Geometry optimization was repeated until the change of the total energy of two adjacent ionic steps was less than 10^{-5} eV and the force on the atoms less than 0.03 eV $Å^{-1}$. To avoid the pseudo interactions between the periodic images along *z* axis, a 15 Å vacuum slab was introduced in each model. For simplicity, Li_2S_4 depicted in Figure S13 (Supporting Information) was employed as the representative polysulfide. Furthermore, to determine the bonding strength between Li_2S_4 and the material surfaces, the adsorption energies ($E_{ad.}$) were defined as

$$E_{ad.} = E_{Li_2S_4/Mat.} - (E_{Li_2S_4} + E_{Mat.}) \quad (2)$$

where $E_{Li_2S_4/Mat.}$ represents the energy of the Li_2S_4 adsorbed on the material surfaces, while $E_{Li_2S_4}$ and $E_{Mat.}$ are the energy of a free Li_2S_4 molecule and that of a material surface.

Supporting Information

Supporting Information is available from the Wiley Online Library or from the author.

Acknowledgements

X.T.G. and Y.X. contributed equally to this work. This work was financially supported by the National Natural Science Foundation of China (Nos. 21676064 and 51633003).

Conflict of Interest

The authors declare no conflict of interest.

Keywords

Li–S batteries, MXene ($Ti_3C_2T_x$), quantum dots, solvothermal synthesis, TiO_2

Received: June 26, 2018
Revised: July 24, 2018
Published online:

[1] a) Q. Pang, X. Liang, C. Y. Kwok, L. F. Nazar, *Nat. Energy* **2016**, *1*, 16132; b) S. Evers, L. F. Nazar, *Acc. Chem. Res.* **2013**, *46*, 1135; c) R. Fang, S. Zhao, Z. Sun, D.-W. Wang, H.-M. Cheng, F. Li, *Adv. Mater.* **2017**, *29*, 1606823; d) H.-J. Peng, J.-Q. Huang, Q. Zhang, *Chem. Soc. Rev.* **2017**, *46*, 5237; e) H. Wang, W. Zhang, H. Liu, Z. Guo, *Angew. Chem., Int. Ed.* **2016**, *55*, 3992; f) A. Manthiram, S.-H. Chung, C. Zu, *Adv. Mater.* **2015**, *27*, 1980.

[2] a) J. Schuster, G. He, B. Mandlmeier, T. Yim, K. T. Lee, T. Bein, L. F. Nazar, *Angew. Chem., Int. Ed.* **2012**, *51*, 3591; b) Z. Zhang, Z. Li, F. Hao, X. Wang, Q. Li, Y. Qi, R. Fan, L. Yin, *Adv. Funct. Mater.* **2014**, *24*, 2500; c) Y. Liu, G. Li, J. Fu, Z. Chen, X. Peng, *Angew. Chem., Int. Ed.* **2017**, *56*, 6176.

[3] a) C. Zhang, H. B. Wu, C. Yuan, Z. Guo, X. W. Lou, *Angew. Chem., Int. Ed.* **2012**, *51*, 9592; b) Z. Li, J. Zhang, B. Guan, D. Wang, L.-M. Liu, X. W. Lou, *Nat. Commun.* **2016**, *7*, 13065; c) C. Ye, L. Zhang, C. Guo, D. Li, A. Vasileff, H. Wang, S.-Z. Qiao, *Adv. Funct. Mater.* **2017**, *27*, 1702524.

[4] a) X.-B. Cheng, J.-Q. Huang, Q. Zhang, H.-J. Peng, M.-Q. Zhao, F. Wei, *Nano Energy* **2014**, *4*, 65; b) H.-J. Peng, W.-T. Xu, L. Zhu, D.-W. Wang, J.-Q. Huang, X.-B. Cheng, Z. Yuan, F. Wei, Q. Zhang, *Adv. Funct. Mater.* **2016**, *26*, 6351; c) G. Hu, Z. Sun, C. Shi, R. Fang, J. Chen, P. Hou, C. Liu, H.-M. Cheng, F. Li, *Adv. Mater.* **2017**, *29*, 1603835.

[5] a) Z. Li, J. Zhang, X. W. Lou, *Angew. Chem., Int. Ed.* **2015**, *54*, 12886; b) L. Qie, A. Manthiram, *Adv. Mater.* **2015**, *27*, 1694.

[6] a) H. Wang, Y. Yang, Y. Liang, J. T. Robinson, Y. Li, A. Jackson, Y. Cui, H. Dai, *Nano Lett.* **2011**, *11*, 2644; b) C. Zu, A. Manthiram, *Adv. Energy Mater.* **2013**, *3*, 1008; c) G. Zhou, L. Li, C. Ma, S. Wang, Y. Shi, N. Koratkar, W. Ren, F. Li, H.-M. Cheng, *Nano Energy* **2015**, *11*, 356; d) R. Fang, S. Zhao, S. Pei, X. Qian, P.-X. Hou, H.-M. Cheng, C. Liu, F. Li, *ACS Nano* **2016**, *10*, 8676; e) J. Cao, C. Chen, Q. Zhao, N. Zhang, Q. Lu, X. Wang, Z. Niu, J. Chen, *Adv. Mater.* **2016**, *28*, 9629; f) B. Papandrea, X. Xu, Y. Xu, C.-Y. Chen, Z. Lin, G. Wang, Y. Luo, M. Liu, Y. Huang, L. Mai, X. Duan, *Nano Res.* **2016**, *9*, 240; g) G. Zhou, E. Paek, G. S. Hwang, A. Manthiram, *Adv. Energy Mater.* **2016**, *6*, 1501355; h) X. Yao, N. Huang, F. Han, Q. Zhang, H. Wan, J. P. Mwizerwa, C. Wang, X. Xu, *Adv. Energy Mater.* **2017**, *7*, 1602923.

[7] a) O. Mashtalir, M. Naguib, V. N. Mochalin, Y. Dall'Agnese, M. Heon, M. W. Barsoum, Y. Gogotsi, *Nat. Commun.* **2013**, *4*, 1716; b) M. Naguib, J. Halim, J. Lu, K. M. Cook, L. Hultman, Y. Gogotsi, M. W. Barsoum, *J. Am. Chem. Soc.* **2013**, *135*, 15966; c) B. Anasori, Y. Xie, M. Beidaghi, J. Lu, B. C. Hosler, L. Hultman, P. R. C. Kent, Y. Gogotsi, M. W. Barsoum, *ACS Nano* **2015**, *9*, 9507; d) J. Halim, S. Kota, M. R. Lukatskaya, M. Naguib, M.-Q. Zhao, E. J. Moon, J. Pitock, J. Nanda, S. J. May, Y. Gogotsi, M. W. Barsoum, *Adv. Funct. Mater.* **2016**, *26*, 3118; e) M. Naguib, O. Mashtalir, J. Carle, V. Presser, J. Lu, L. Hultman, Y. Gogotsi, M. W. Barsoum, *ACS Nano* **2012**, *6*, 1322; f) M. Naguib, M. Kurtoglu, V. Presser, J. Lu, J.-J. Niu, M. Heon, L. Hultman, Y. Gogotsi, M. W. Barsoum, *Adv. Mater.* **2011**, *23*, 4248; g) M. Naguib, V. N. Mochalin, M. W. Barsoum, Y. Gogotsi, *Adv. Mater.* **2014**, *26*, 992; h) W. Bao, X. Tang, X. Guo, S. Choi, C. Wang, Y. Gogotsi, G. Wang, *Joule* **2018**, *2*, 778.

[8] a) B. Anasori, M. R. Lukatskaya, Y. Gogotsi, *Nat. Rev. Mater.* **2017**, *2*, 16098; b) K. Maleski, V. N. Mochalin, Y. Gogotsi, *Chem. Mater.* **2017**, *29*, 1632; c) M. A. Hope, A. C. Forse, K. J. Griffith, M. R. Lukatskaya, M. Ghidiu, Y. Gogotsi, C. P. Grey, *Phys. Chem. Chem. Phys.* **2016**, *18*, 5099.

[9] a) X. Sang, Y. Xie, M.-W. Lin, M. Alhabeb, K. L. Van Aken, Y. Gogotsi, P. R. C. Kent, K. Xiao, R. R. Unocic, *ACS Nano* **2016**, *10*, 9193; b) A. D. Dillon, M. J. Ghidiu, A. L. Krick, J. Griggs, S. J. May, Y. Gogotsi, M. W. Barsoum, A. T. Fafarman, *Adv. Funct. Mater.* **2016**, *26*, 4162; c) B. Anasori, C. Shi, E. J. Moon, Y. Xie, C. A. Voigt, P. R. C. Kent, S. J. May, S. J. L. Billinge, M. W. Barsoum, Y. Gogotsi, *Nanoscale Horiz.* **2016**, *1*, 227; d) M. Mariano, O. Mashtalir, F. Q. Antonio, W.-H. Ryu, B. Deng, F. Xia, Y. Gogotsi, A. D. Taylor, *Nanoscale* **2016**, *8*, 16371.

[10] a) D. Xiong, X. Li, Z. Bai, S. Lu, *Small* **2018**, *14*, 1703419; b) S. Cao, B. Shen, T. Tong, J. Fu, J. Yu, *Adv. Funct. Mater.* **2018**, *28*, 1800136; c) Q. Tang, Z. Zhou, P. Shen, *J. Am. Chem. Soc.* **2012**, *134*, 16909.

[11] a) X. Liang, A. Garsuch, L. F. Nazar, *Angew. Chem., Int. Ed.* **2015**, *54*, 3907; b) W. Bao, L. Liu, C. Wang, S. Choi, D. Wang, G. Wang, *Adv. Energy Mater.* **2018**, *8*, 1702485.

[12] a) V. N. Borysiuk, V. N. Mochalin, Y. Gogotsi, *Nanotechnology* **2015**, *26*, 265705; b) V. N. Borysiuk, V. N. Mochalin, Y. Gogotsi, *Comput. Mater. Sci.* **2018**, *143*, 418.

[13] a) W. Bao, D. Su, W. Zhang, X. Guo, G. Wang, *Adv. Funct. Mater.* **2016**, *26*, 8746; b) W. Bao, X. Xie, J. Xu, X. Guo, J. Song, W. Wu, D. Su, G. Wang, *Chem. - Eur. J.* **2017**, *23*, 12613; c) X. Liang, Y. Rangom, C. Y. Kwok, Q. Pang, L. F. Nazar, *Adv. Mater.* **2017**, *29*, 1603040.

[14] a) Z. W. Seh, W. Li, J. J. Cha, G. Zheng, Y. Yang, M. T. McDowell, P.-C. Hsu, Y. Cui, *Nat. Commun.* **2013**, *4*, 1331; b) J. Li, B. Ding, G. Xu, L. Hou, X. Zhang, C. Yuan, *Nanoscale* **2013**, *5*, 5743; c) H. Wang, S. Li, D. Li, Z. Chen, H. K. Liu, Z. Guo, *Energy* **2014**, *75*, 597; d) X. Liang, C. Y. Kwok, F. Lodi-Marzano, Q. Pang, M. Cuisinier, H. Huang, C. J. Hart, D. Houtarde, K. Kaup, H. Sommer, T. Brezesinski, J. Janek, L. F. Nazar, *Adv. Energy Mater.* **2016**, *6*, 1501636; e) S. Evers, T. Yim, L. F. Nazar, *J. Phys. Chem. C* **2012**, *116*, 19653.

[15] a) M. Yu, J. Ma, H. Song, A. Wang, F. Tian, Y. Wang, H. Qiu, R. Wang, *Energy Environ. Sci.* **2016**, *9*, 1495; b) Z. Xiao, Z. Yang, L. Wang, H. Nie, M. Zhong, Q. Lai, X. Xu, L. Zhang, S. Huang, *Adv. Mater.* **2015**, *27*, 2891; c) Q. Pang, D. Kundu, M. Cuisinier, L. F. Nazar, *Nat. Commun.* **2014**, *5*, 4759; d) Y. Wang, X. Huang, S. Zhang, Y. Hou, *Small Methods* **2018**, *2*, 1700345; e) Y. Chen, S. Choi, D. Su, X. Gao, G. Wang, *Nano Energy* **2018**, *47*, 331.

[16] M.-Q. Zhao, M. Torelli, C. E. Ren, M. Ghidiu, Z. Ling, B. Anasori, M. W. Barsoum, Y. Gogotsi, *Nano Energy* **2016**, *30*, 603.

[17] a) X. Wu, Z. Wang, M. Yu, L. Xiu, J. Qiu, *Adv. Mater.* **2017**, *29*, 1607017; b) B. Ahmed, D. H. Anjum, Y. Gogotsi, H. N. Alshareef, *Nano Energy* **2017**, *34*, 249.

[18] a) C. Zhang, S. J. Kim, M. Ghidiu, M.-Q. Zhao, M. W. Barsoum, V. Nicolosi, Y. Gogotsi, *Adv. Funct. Mater.* **2016**, *26*, 4143; b) M. Naguib, O. Mashtalir, M. R. Lukatskaya, B. Dyatkin, C. Zhang, V. Presser, Y. Gogotsi, M. W. Barsoum, *Chem. Commun.* **2014**,

50, 7420; c) Z. Li, H. Zhang, J. Han, Y. Chen, H. Lin, T. Yang, *Adv. Mater.* **2018**, *30*, 1706981.

[19] a) W. Li, F. Wang, Y. Liu, J. Wang, J. Yang, L. Zhang, A. A. Elzatahry, D. Al-Dahyan, Y. Xia, D. Zhao, *Nano Lett.* **2015**, *15*, 2186; b) B. Qiu, M. Xing, J. Zhang, *J. Am. Chem. Soc.* **2014**, *136*, 5852; c) Z. Wang, J. Sha, E. Liu, C. He, C. Shi, J. Li, N. Zhao, *J. Mater. Chem. A* **2014**, *2*, 8893; d) S. Ding, J. S. Chen, D. Luan, F. Y. C. Boey, S. Madhavi, X. W. Lou, *Chem. Commun.* **2011**, *47*, 5780.

[20] Y.-T. Liu, P. Zhang, N. Sun, B. Anasori, Q.-Z. Zhu, H. Liu, Y. Gogotsi, B. Xu, *Adv. Mater.* **2018**, *30*, 1707334.

[21] X. Zhao, M. Liu, Y. Chen, B. Hou, N. Zhang, B. Chen, N. Yang, K. Chen, J. Li, L. An, *J. Mater. Chem. A* **2015**, *3*, 7870.

[22] T. Zhou, W. Lv, J. Li, G. Zhou, Y. Zhao, S. Fan, B. Liu, B. Li, F. Kang, Q.-H. Yang, *Energy Environ. Sci.* **2017**, *10*, 1694.

[23] a) S. Kajiyama, L. Szabova, K. Sodeyama, H. Iinuma, R. Morita, K. Gotoh, Y. Tateyama, M. Okubo, A. Yamada, *ACS Nano* **2016**, *10*, 3334; b) X. Xie, M.-Q. Zhao, B. Anasori, K. Maleski, C. E. Ren, J. Li, B. W. Byles, E. Pomerantseva, G. Wang, Y. Gogotsi, *Nano Energy* **2016**, *26*, 513.

[24] R. Mo, Z. Lei, K. Sun, D. Rooney, *Adv. Mater.* **2014**, *26*, 2084.

[25] a) Y. Liang, D. Wu, X. Feng, K. Müllen, *Adv. Mater.* **2009**, *21*, 1679; b) H.-J. Shin, K. K. Kim, A. Benayad, S.-M. Yoon, H. K. Park, I.-S. Jung, M. H. Jin, H.-K. Jeong, J. M. Kim, J.-Y. Choi, Y. H. Lee, *Adv. Funct. Mater.* **2009**, *19*, 1987.

[26] Z. Fan, K. Wang, T. Wei, J. Yan, L. Song, B. Shao, *Carbon* **2010**, *48*, 1686.

[27] M. J. Fernández-Merino, L. Guardia, J. I. Paredes, S. VillarRodil, P. Solís-Fernández, A. Martínez-Alonso, J. M. D. Tascón, *J. Phys. Chem. C* **2010**, *114*, 6426.

[28] M. Ghidiu, M. R. Lukatskaya, M.-Q. Zhao, Y. Gogotsi, M. W. Barsoum, *Nature* **2014**, *516*, 78.

[29] a) F. Shahzad, M. Alhabeb, C. B. Hatter, B. Anasori, S. M. Hong, C. M. Koo, Y. Gogotsi, *Science* **2016**, *353*, 1137; b) Z. Lin, D. Barbara, P.-L. Taberna, K. L. Van Aken, B. Anasori, Y. Gogotsi, P. Simon, *J. Power Sources* **2016**, *326*, 575; c) B. Xu, M. Zhu, W. Zhang, X. Zhen, Z. Pei, Q. Xue, C. Zhi, P. Shi, *Adv. Mater.* **2016**, *28*, 3333; d) Q. Xue, H. Zhang, M. Zhu, Z. Pei, H. Li, Z. Wang, Y. Huang, Y. Huang, Q. Deng, J. Zhou, S. Du, Q. Huang, C. Zhi, *Adv. Mater.* **2017**, *29*, 1604847.

[30] C. Peng, X. Yang, Y. Li, H. Yu, H. Wang, F. Peng, *ACS Appl. Mater. Interfaces* **2016**, *8*, 6051.

[31] a) G. Kresse, J. Hafner, *Phys. Rev. B* **1993**, *47*, 558; b) G. Kresse, J. Hafner, *Phys. Rev. B* **1994**, *49*, 14251; c) G. Kresse, J. Furthmüller, *Phys. Rev. B* **1996**, *54*, 11169; d) G. Kresse, J. Furthmüller, *Comput. Mater. Sci.* **1996**, *6*, 15.

[32] a) E. S. Sim, G. S. Yi, M. Je, Y. Lee, Y.-C. Chung, *J. Power Sources* **2017**, *342*, 64; b) E. S. Sim, Y.-C. Chung, *Appl. Surf. Sci.* **2018**, *435*, 210.

[33] a) R. Dronskowski, P. E. Bloechl, *J. Phys. Chem.* **1993**, *97*, 8617; b) S. Maintz, V. L. Deringer, A. L. Tchougréeff, R. Dronskowski, *J. Comput. Chem.* **2013**, *34*, 2557.

[34] Z. Deng, Z. Zhang, Y. Lai, J. Liu, J. Li, Y. Liu, *J. Electrochem. Soc.* **2013**, *160*, A553.

[35] J. Chmiola, C. Largeot, P. L. Taberna, P. Simon, Y. Gogotsi, *Science* **2010**, *328*, 480.

[36] H.-J. Peng, G. Zhang, X. Chen, Z.-W. Zhang, W.-T. Xu, J.-Q. Huang, Q. Zhang, *Angew. Chem., Int. Ed.* **2016**, *55*, 12990.

[37] Z. Zhang, L.-L. Kong, S. Liu, G.-R. Li, X.-P. Gao, *Adv. Energy Mater.* **2017**, *7*, 1602543.

[38] X. Wu, Y. Du, P. Wang, L. Fan, J. Cheng, M. Wang, Y. Qiu, B. Guan, H. Wu, N. Zhang, K. Sun, *J. Mater. Chem. A* **2017**, *5*, 25187.

[39] a) P. E. Blöchl, *Phys. Rev. B* **1994**, *50*, 17953; b) J. P. Perdew, K. Burke, M. Ernzerhof, *Phys. Rev. Lett.* **1996**, *77*, 3865.